#### 1

# Security-Constrained Unit Commitment Considering Locational Frequency Stability in Low-Inertia Power Grids

Mingjian Tuo, Student Member, IEEE and Xingpeng Li, Member, IEEE

Abstract—With increasing installation of wind and solar generation, conventional synchronous generators in power systems are gradually displaced resulting in a significant reduction in system inertia. Maintaining system frequency within acceptable ranges becomes more critical for the stability of a power system. In this paper, we first study the impact of inter-area oscillations on the system rate-of-change-of-frequency (RoCoF) security; then, the limitations on locational RoCoFs accounting for G-1 contingency stability are derived. By enforcing these frequency related constraints, a location based RoCoF constrained security constrained unit commitment (LRC-SCUC) model is proposed. Furthermore, an effective piecewise linearization (PWL) technique is employed to formulate a RoCoF linearization problem and linearize the nonlinear function representing the location based RoCoF constraints in SCUC. Simulation results reveal that the inclusion of inertia-related constraints can substantially improve the system stability at the cost of higher operation cost. The results also show that deploying virtual inertia techniques not only reduces the total cost, but also improves the system market efficiency.

Index Terms— Energy Markets, Frequency stability, Inertia distribution, Linear programming, Low-inertia grid, Optimization, Security-constrained unit commitment, Virtual Inertia.

# Nomenclature

	NOMENCLATURE
Sets	
G	Set of online generators.
$G_n$	Set of online generators connected to bus $n$ .
$G_l$	Set of online generators on local buses.
$G_{nl}$	Set of online generators on non-local buses.
K	Set of lines.
$K^+(n)$	Set of lines with bus <i>n</i> as receiving bus.
$K^-(n)$	Set of lines with bus <i>n</i> as sending bus.
T	Set of time periods.
N	Set of buses.
$N_l$	Set of local buses adjacent to the event.
$N_{nl}$	Set of non-local buses distant to the event.
Indices	
g	Generator g.
k	Line k.
t	Time <i>t</i> .
n	Bus $n$ .

#### **Parameters**

$c_g$	Linear operation cost for generator $g$ .
$P_g^{min}$	Minimum output limit of generator g.
$P_q^{max}$	Maximum output limit of generator g.
$P_{\nu}^{max}$	Long-term thermal line limit for line <i>k</i> .

Mingjian Tuo and Xingpeng Li are with the Department of Electrical and Computer Engineering, University of Houston, Houston, TX, 77204, USA (e-mail: mtuo@uh.edu; Xingpeng.Li@asu.edu).

$d_{n,t}$	Forecasted demand at bus $n$ in period $t$ .
$E_{n,t}$	Forecasted renewable generation at bus $n$ in period $t$ .
$R_q^{hr}$	Ramp limit of generator g.
$R_g^{re}$	Reserve capacity of generator g.
$H_g$	Inertia constant of conventional generator g.
$c_g^{ar{N}L}$	No load cost for generator g.
$c_g^{SU}$	Startup cost of generator g.
$c_g^{RE}$	Reserve cost of generator g.
$c_n$	Nodal cost for additional inertia at bus $n$ .
$\Delta t$	Frequency monitoring window.
$T_1$	First frequency measuring interval.
$T_2$	Second frequency measuring interval.

Susceptance of line k.

#### **Variables**

, cirtuo i co	
$P_{g,t}$	Output of generator $g$ in period $t$ .
$m_t$	Average nodal inertia in period $t$ .
$\Delta m_{g,t}$	Change in post-contingency average nodal inertia in
	period t.
$r_{n,t}$	Output of renewables of bus $n$ in period $t$ .
$r_{g,t}$	Ramp power of generator $g$ in period $t$ .
$u_{g,t}$	Commitment status of generator g in period t.
$v_{g,t}$	Start-up variable of generator g in period t.
$M_t$	System aggregate inertia in period <i>t</i> .
$M_t^{VI}$	Virtual inertia in period <i>t</i> .
$P_{k,t}$	Flow online $k$ in period $t$ .
$\theta_{n,t}$	Phase angle of bus $n$ in period $t$ .
$\theta_{m,t}$	Phase angle of bus $m$ in period $t$ .

# I. INTRODUCTION

Renewable energy sources (RES) have become the promising technology to meet the demand for the reduction of the CO<sub>2</sub> emissions. Within the next few decades, generation with synchronous generators will gradually be replaced by converter-connected renewable energy sources such as wind and solar generations. As a result of this transition, current power system may ultimately shift towards a 100% converter-based power system [1]. Traditionally, synchronous generators provide inertia through stored kinetic energy in rotating mass which can counteract frequency excursion during disturbances and thus enhance the frequency stability. While RESs are interfaced to the grid through converters which electrically decouples the rotor's inertia from the whole system [2], contributing little synchronous inertia to the whole system, which is even true for wind power plants taking advantage of kinetic energy stored in wind turbines.

With more generation coming from converter-based resources, insufficient inertia would be a main challenge for power systems stability. Moreover, low inertia feature together with variable renewable generation characteristics may lead to

high rate of change of frequency (RoCoF) and large frequency excursion. When RoCoF or frequency deviation exceeds certain thresholds, protection devices would disconnect generators from the grid [3]. On August 9, 2019, over 1 million customers were affected by a major power disruption (mainly came from offshore wind farms) that occurred across England and Wales and some parts of Scotland and the frequency of the system hit 48.8 Hz [4]. The impact of RESs integration on power systems has been studied to address frequency stability challenge. In [5], the authors explored the massive deployment of grid-forming converters and its effects on frequency stability, results show that the system stability is lost when converter-based resources penetration reaches 80%. The Electric Reliability Council of Texas (ERCOT) studied the effect of low inertia on grid security and reliability [6]-[7]. To improve the frequency control for systems with high renewable energy penetration level, several regulation methods have been proposed. In [7], a fuzzy based wind hybrid energy storage system has been proposed to suppress the power fluctuation. Recently, the enhanced frequency response has been introduced in Great Britain which includes technologies like battery storage, interconnectors, and demand response [8]. Frequency control ancillary services have been implemented in the Australian National Electricity Market to maintain the system stability [9].

Following a different approach, several transmission system operators have imposed extra inertia constraints in the security-constrained unit commitment (SCUC) model to keep the minimum amount of synchronous inertia online [10]. EirGrid has introduced a synchronous inertial response (SIR) constraint to ensure that the available inertia does not fall below a static limit of 23,000 MWs in Ireland [11]. In [12], the authors introduced frequency-related constraints in SCUC: enforcing limitations on RoCoF, frequency nadir and steady-state error that are derived from a uniform frequency response model. A novel mixed-integer linear programming (MILP) unit commitment formulation was proposed in [13], which simultaneously optimizes energy production and the allocation of inertia. These studies showcase the benefits in terms of system frequency stability from including frequency related constraints in the SCUC model.

Different from focusing on the collective performance of the power system, the RoCoF experienced by each bus is distinct. [5] and [14] show that generators on the buses adjacent to the event may suffer higher RoCoFs. It is also observed in [15] that the relative location of measurement point to disturbance is a pertinent factor in system inertial response and the RoCoF is usually higher for location where networks are weakly interconnected. In [16], network coherency was considered as an alternative performance metric, and a system dynamic model was formulated to determine the allocation of additional inertia based on the disturbance location and nodal frequency deviation. However, these prior studies neglect the impact of disturbance propagation on post-contingency frequency dynamics and fail to consider locational frequency security in SCUC models. In addition, the sensitivity analysis of RES penetration level and the impact of virtual inertia have not been discussed thoroughly.

In this article, we aim to bridge the aforementioned research gaps. The main contributions are summarized below:

- First, the impact of disturbance propagation on system dynamics is investigated. In contrast to existing literatures such as [17] where only system equivalent model based RoCoF constrained SCUC (ERC-SCUC) are studied, we propose a novel location based RoCoF constrained SCUC (LRC-SCUC) model that can counteract the impact of system oscillation and guarantee the locational RoCoF security following a *G*-1 disturbance.
- Three different SCUC models, (a) a traditional SCUC (T-SCUC) model without any RoCoF constraints, (b) existing ERC-SCUC model, and (c) the proposed LRC-SCUC model, are examined and compared. Simulation results demonstrate the performance of the proposed LRC-SCUC model in terms of system frequency stability under contingency.
- A piecewise linearization (PWL) based method is proposed to convert the non-linear frequency constraints into linear frequency constraints in the proposed LRC-SCUC model, which allows us to optimally schedule the synchronous inertia as well as inertial services provided by nonsynchronous resources to meet the minimum system inertia requirement for power systems with higher RES integration.
- Moreover, we propose two virtual inertia based LRC-SCUC (VI-LRC-SCUC) and ERC-SCUC (VI-ERC-SCUC) models to examine the effect of virtual inertia. Case studies show virtual inertia techniques can reduce the total cost by avoiding unnecessary commitment of extra expensive synchronous generators while meeting the system inertia requirement.
- Last, the energy market results demonstrate that imposing RoCoF constraints would increase the operational cost, load payment, and congestion revenue. Incorporating virtual inertia can largely reduce the system overall congestion and improve the market efficiency of the proposed LRC-SCUC model.

The remaining part of this paper is organized as follows. In Section II, we derive the post-contingency frequency dynamics and incorporate the corresponding analytic expressions into the SCUC model. Section III investigates the *G*-1 contingencies at different locations to implement the non-linear location based RoCoF constraints, and the PWL method is utilized to linearize those non-linear location based RoCoF constraints. Section IV presents the proposed LRC-SCUC model and VI-LRC-SCUC model, as well as the T-SCUC, ERC-SCUC and VI-ERC-SCUC as benchmark models. Case studies are presented in Section V. Finally, Section VI draws the main conclusions and describes potential future work.

#### II. SYSTEM FREQUENCY DYNAMICS MODEL

The synchronous generator provides inertia to the power system through strongly coupled mechanical dynamics and electrical dynamics. Following a sudden change in load or a generation contingency, the dynamic behavior of the system frequency can be described using the swing equation of system equivalent single-machine representation,

$$P_m - P_e = M \frac{d \triangle \omega}{dt} + D \triangle \omega \tag{1}$$

where M and D are the aggregated system inertia constant and damping coefficient corresponding to the committed synchro-

nous generators respectively.  $P_m$  is the mechanical input power.  $P_e$  is the electrical output power.

The transmission network can be considered as a graph consisting of nodes (buses) and edges (branches). Using the topological information and the system parameters, the swing equation can then be extended and reformulated to describe the oscillatory behavior of each individual bus as follows,

$$m_i \ddot{\theta}_i + d_i \dot{\theta}_i = p_{in,i} - p_{e,i}, \quad i \in \{1, ..., n\}$$
 (2)

where  $m_i$  and  $d_i$  denote the inertia coefficients and damping ratio for node i respectively, while  $p_{in,i}$  and  $p_{e,i}$  refer to the input power and output power respectively. Under the same assumption with DC power flow model, the electrical output power  $p_{e,i}$  at bus i is only related to the voltage phase angles as illustrated by (3).

$$p_{e,i} = \sum_{i=1}^{n} b_{ij} (\theta_i - \theta_j), \ i \in \{1, ..., n\}$$
 (3)

By substituting (3) into (2) and then eliminating passive load buses via Kron reduction [18], we can obtain a networkreduced model with N generator buses. Then, the phase angle  $\theta$  of generator buses can be expressed by the following dynamic equation,

$$M\ddot{\theta} + D\dot{\theta} = P - L\theta \tag{4}$$

where  $M = \text{diag}(\{m_i\})$ ,  $D = \text{diag}(\{d_i\})$ . The linear approximation (3) can be justified since the angle difference of the voltage phasors are small; thus for the Laplacian matrix L of the grid, its off-diagonal elements are  $l_{ij} = -b_{ij}V_i^{(0)}V_i^{(0)}$  and diagonals are  $l_{ii} = \sum_{j=1, j\neq i}^{n} b_{ij} V_i^{(0)} V_j^{(0)}$ . In this paper, the Laplacian matrix of the network-reduced model is real and symmetric [19], which has a complete orthogonal set of eigenvectors  $\{\beta_{\alpha}\}$  with eigenvalue  $\{\lambda_{\alpha}\}$ . The properties of symmetric Laplacian matrix imply that  $\lambda_1 = 0$ , corresponding to an eigenvalue  $\lambda_1 = 0$ genvector with constant components,  $\{(\beta_1)^T = \frac{1,...,1}{\sqrt{N}}\}$ . Higher eigenvalues  $\lambda_{\alpha}$  of L are positive for  $\alpha = 2, ..., N$ . Under the assumption of homogeneous inertia coefficient without inertia heterogeneity effect, frequency deviations at bus i can be derived [20],

$$\delta\dot{\theta}_{i}(t) = \frac{\Delta P e^{-\frac{\gamma t}{2}}}{m} \sum_{\alpha=1}^{N} (\beta_{\alpha i} \beta_{\alpha b} \frac{\sin\left(\sqrt{\frac{\lambda_{\alpha}}{m} - \frac{\gamma^{2}}{4}}t\right)}{\sqrt{\frac{\lambda_{\alpha}}{m} - \frac{\gamma^{2}}{4}}})$$
(5)

where m denotes average inertia over generator buses; and bus b is the location where disturbance occurs. The ratio of damping coefficient to inertia coefficient usually strictly prescribed within narrow ranges,  $\gamma = d_i/m_i$ , which is assumed as a constant. As the frequency is monitored at discrete time interval, we consider a time interval length of  $\Delta t$ , then RoCoF on bus i,  $R_i(t)$ , can be calculated as:

$$R_{i}(t) = \frac{\delta \dot{\theta}_{i}(t + \Delta t) - \delta \dot{\theta}_{i}(t)}{2\pi \Delta t}$$
 After we substitute (5) into (6), we can obtain,

$$R_{i}(t) = \frac{\Delta P e^{-\frac{\gamma t}{2}}}{2\pi m} \sum_{\alpha=1}^{N} \frac{\beta_{\alpha i} \beta_{\alpha b}}{\frac{\lambda_{\alpha}}{\lambda_{\alpha}} \frac{\gamma^{2}}{2}} e^{-\frac{\gamma \Delta t}{2}} \sin\left(\sqrt{\frac{\lambda_{\alpha}}{m} - \frac{\gamma^{2}}{4}}(t + \frac{\gamma^{2}}{2})\right)$$
(7)

$$\Delta t)$$
  $-\sin\left(\sqrt{\frac{\lambda_{\alpha}}{m}-\frac{\gamma^2}{4}}t\right)$ 

The term corresponding to  $\alpha = 1$  in (7) can be simplified as (8). It is observed that term  $\alpha = 1$  gives a positionindependent contribution to the RoCoF which is inversely proportional to the inertia coefficient m.

$$R_i^{(1)}(t) = \frac{\Delta P e^{-\gamma t} (1 - e^{-\gamma \Delta t})}{2N\pi m \nu \Delta t}$$
 (8)

The initial inertial response can then be calculated as,

$$\lim_{\Delta t \to 0, \ t \to 0} R_i^{(1)}(t) = \frac{\Delta P}{2\pi N m}$$
 (9)

which corresponds to the system inertia response. From (7) and (9), it can be observed that the nodal inertia distribution plays a vital role in the first few seconds; a higher inertia density results in a lower RoCoF, which allows longer responding time for the primary control to act.

Results in [20] suggest that all other terms  $\alpha > 1$  have oscillations with both amplitude and period depending on  $\sqrt{\lambda_{\alpha}/m - \gamma^2/4}$ . Therefore, high-lying eigenmodes and eigenvalues  $\lambda_{\alpha}$  with  $\alpha \geq 3$  contribute much less than the second slowest eigenmode, i.e. the Fielder mode, of the system Laplacian matrix L. For the IEEE 24-bus system case,  $\sqrt{\lambda_3/m - \gamma^2/4}$  is four times larger than  $\sqrt{\lambda_2/m - \gamma^2/4}$ . Hence, we only consider the RoCoF contributions from terms  $\alpha \leq 2$ . The simplified but effective function to calculate nodal RoCoF can be given as follows,

$$R_{i}^{(1,2)}(t) = \frac{\Delta P e^{-\gamma \frac{t}{2}} (1 - e^{-\gamma \Delta t})}{2N\pi m \gamma \Delta t} + \frac{\Delta P e^{-\gamma \frac{t}{2}}}{2\pi m} \frac{\beta_{2i} \beta_{2b}}{\sqrt{\frac{\lambda_{2}}{m} - \frac{\gamma^{2}}{4}} \Delta t}$$

$$\left[ e^{-\gamma \frac{\Delta t}{2}} \sin\left(\sqrt{\frac{\lambda_{2}}{m} - \frac{\gamma^{2}}{4}} (t + \Delta t)\right) - \sin\left(\sqrt{\frac{\lambda_{2}}{m} - \frac{\gamma^{2}}{4}} t\right) \right]$$
(10)

Research in [21] has shown that RoCoF experienced by different generators can be different depending on their inertia constant and electrical distance from the disturbance. By monitoring the average frequency change, the RoCoF relays can make more secure decisions during contingency. Practically, the time interval or measuring window for calculating RoCoF ranges from 5 cycles to 10 cycles [22]. In this paper, the average frequency change over a period of 100 ms (6 cycles) is defined as the RoCoF value.

#### III. FORMULATION OF FREQUENCY CONSTRAINTS

This section investigates the linearization problem of locational RoCoF constraints considering frequency evolution following a potential G-1 contingency in the system. We first define the contingency that will be considered in this paper. Compared to the case of a sudden load increase, the loss of generation not only causes mismatch in system power balance, but also decreases the system synchronous inertia resulting in higher frequency deviation and larger initial RoCoF. Thus, the G-1 contingency of largest generation is considered as the worst contingency in this study.

Due to the impact of inter-area oscillations, the actual need for frequency ancillary services would usually be underestimated [23], generators in some areas would then suffer much higher RoCoF and have a higher chance to get tripped [24]. To investigate how Fiedler mode affects the locational frequency response and the relating ancillary services, simulations are conducted on the IEEE 24-bus system with a step increase of 180 MW load. With assumption of small differences in phase angles, Fig. 1 shows the distribution of Fiedler mode of the Laplacian matrix corresponding to the reduced network of the IEEE 24-bus system via Kron reduction. Comparing to the original full model, the Fiedler mode of the reduced model manifests the frequency dynamics of individual generator bus more accurately [25]. Fig. 2 shows that the frequency response curves of bus 13 and bus 23 are close to the curve of center of inertia (COI) [25] over the whole monitoring course, implying relatively less oscillation amplitude, while the largest oscillation is observed on bus 7 that corresponds to the highest Fiedler mode.

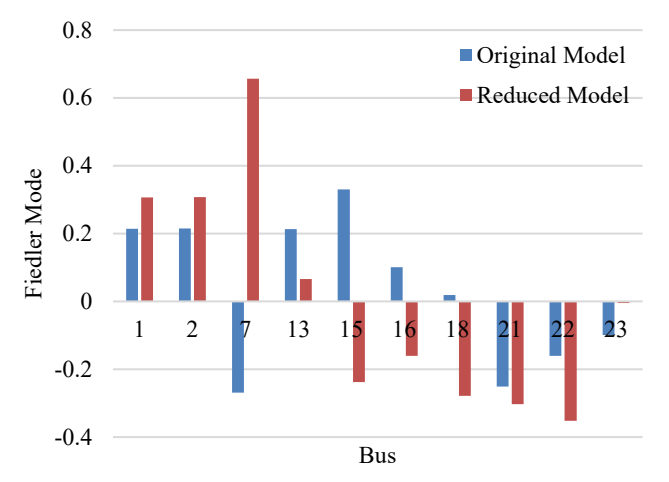
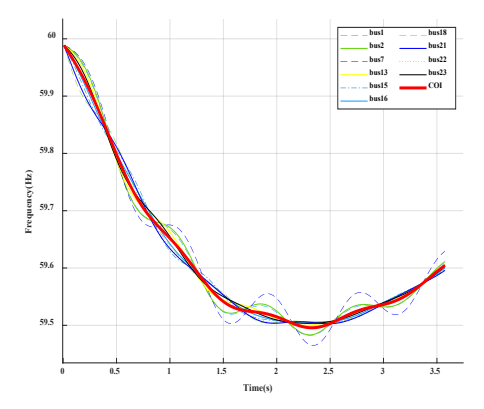


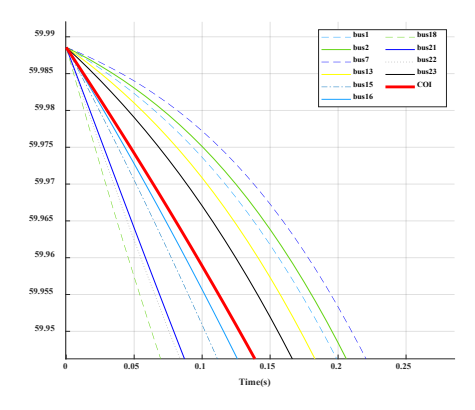
Fig. 1. Fiedler mode distribution.

Results in [20] and [5] suggest that generators adjacent to the event usually perceive highest RoCoF earlier comparing to the generators on distant buses. Thus, we define the set of buses adjacent to the event of a sudden change in demand or *G*-1 contingency as local buses, while the rest buses distant to the event are defined as non-local buses. The distribution of Fiedler mode can help determine the local and non-local buses. From the expression (10) we derived, it can be inferred that buses sharing the same positive or negative Fiedler mode with the event bus are considered local buses. Generators on local buses are most likely to perceive highest RoCoF before COI frequency, while the generators on non-local buses may perceive highest RoCoF later than the COI frequency.

The simulation results shown in Fig. 2 also support the aforementioned inference. It can be observed that, following an event, there are faster frequency excursions and higher RoCoF especially for the generators on local buses adjacent to the disturbance comparing to COI frequency; for generators on non-local buses, highest RoCoF occurs later than COI frequency with a time period delay.



(a) Frequency for period between t=0 and t=3.5s



(b) Frequency for the period between *t*=0s and *t*=0.25s. Fig. 2. Frequency response following a disturbance on bus 18.

To guarantee the locational frequency security for all buses and limit the highest RoCoF, the aforementioned RoCoF expression in (10) are incorporated as constraints in SCUC. The resulting locational RoCoF constraint (11) that respects the prescribed threshold RoCoF<sub>lim</sub> is then reformulated as follows with t being set as  $T_1$  for local buses or  $T_2$  for non-local buses which are mostly determined by the electrical interconnection of the power system [23].

$$\frac{\Delta P e^{-\gamma \frac{t}{2}} (1 - e^{-\gamma \Delta t})}{2N\pi (m - \Delta m)\gamma \Delta t} + \frac{\Delta P e^{-\gamma \frac{t}{2}}}{2\pi (m - \Delta m)} \frac{\beta_{2i}\beta_{2b}}{\sqrt{\frac{\lambda_2}{m - \Delta m} \frac{\gamma^2}{4} \Delta t}}$$

$$\left[ e^{-\gamma \frac{\Delta t}{2}} \sin \left( \sqrt{\frac{\lambda_2}{m - \Delta m} - \frac{\gamma^2}{4}} (t + \Delta t) \right) - \sin \left( \sqrt{\frac{\lambda_2}{m - \Delta m} - \frac{\gamma^2}{4}} t \right) \right] \leq RoCoF_{lim}$$
(11)

where  $\Delta m$  denotes an average loss of inertia coefficient distributed on each bus. Within a plausible range of variables  $(\Delta P, m, \Delta m, \gamma)$ , the RoCoF on all buses including local buses and non-local buses following a G-1 contingency can be calculated with the left-hand side terms of (11). The constraints on RoCoF for locational frequency dynamics are nonlinear. In order to incorporate these frequency-related constraints into the proposed LRC-SCUC model, a linear approximation method is introduced. The study in [26] proposes a piece-wise linearization technique for obtaining a linearized expression. Since respective damping and droop gains are usually strictly prescribed proportional to the synchronous inertia, the RoCoF expression becomes a function of three variables  $R_i^{(1,2)}(\Delta P, m, \Delta m)$  that can be expressed as  $a_v\Delta P + b_vm +$ 

 $c_v \Delta m + d_v$ . In order to determine these four coefficients, we need to formulate and solve the problem.

The least squares based PWL method aims to minimize the following objective function,

$$\min_{\Psi} \sum_{\eta} \left( \max_{1 \le \nu \le \overline{\nu}} \{ a_{\nu} \Delta P + b_{\nu} m + c_{\nu} \Delta m + d_{\nu} \} - R_{i}^{(1,2)}(\Delta P, m, \Delta m) \right)^{2}$$

$$(12)$$

where  $\Psi = \{a_v, b_v, c_v, d_v, \forall v\}$  is the set of parameters to be determined;  $\eta$  denotes the evaluation point;  $\nu$  refers to the index of PWL segments and  $\bar{v}$  denotes the number of PWL segments. The problem of fitting  $\max_{1 \le \nu \le \bar{\nu}} \{a_\nu \Delta P + b_\nu m +$ 

 $c_v \Delta m + d_v$  to  $R_i^{(1,2)}(\Delta P, m, \Delta m)$  over the plausible range can be considered as minimizing difference between the appropriate PWL segment and the RoCoF function. To solve this minmax problem and eliminate the inner max operator from the objective function, new variables  $t_n$  are introduced and defined as follows,

$$t_1 = \max \{ a_1 \Delta P + b_1 m + c_1 \Delta m + d_1, a_2 \Delta P + b_2 m + c_2 \Delta m + d_2 \}.$$
 (13a)

$$a_{2}\Delta P + b_{2}m + c_{2}\Delta m + d_{2} \},$$

$$t_{\nu-1} = max\{t_{\nu-2}, a_{\nu}\Delta P + b_{\nu}m + c_{\nu}\Delta m + d_{\nu}\}, 3 \le \nu \le \bar{\nu}.$$
(13a)

Adding new linear inequalities would relieve the objective function from the "max" operator [26]. We basically introduce  $\bar{v} - 1$  new binary  $\alpha_v$  as well as  $\bar{v} - 1$  continuous variables  $t_v$ , the unconstrained min-max optimization problem (12) can be reformulated as a constrained optimization problem (14)-(15), which is the RoCoF linearization problem.

$$\min_{\Psi} \sum_{\eta} \left( t_{\bar{v}-1}(\Delta P, m, \Delta m) - R_i^{(1,2)}(\Delta P, m, \Delta m) \right)^2$$
 (14)

subject to the following constraints.

$$a_1 \Delta P + b_1 m + c_1 \Delta m + d_1 \le t_1 \le a_1 \Delta P + b_1 m + c_1 \Delta m + d_1 + \alpha_1 \Omega, \ \forall \eta,$$

$$(15a)$$

$$a_2 \Delta P + b_2 m + c_2 \Delta m + d_2 \le t_1 \le a_2 \Delta P + b_2 m + c_2 \Delta m + d_2 + (1 - \alpha_1) \Omega, \quad \forall n,$$
 (15b)

$$t_{v-2} \le t_{v-1} \le t_{v-2} + \alpha_{v-1} \Omega, \quad \forall \eta, 3 \le v \le \bar{v},$$
 (15c)

$$a_n \Delta P + b_n m + c_n \Delta m + d_n \le t_{n-1} \le a_n \Delta P + a_n \Delta P$$

$$b_n m + c_n \Delta m + d_n + (1 - \alpha_{n-1}) \Omega_n$$
 (15d)

$$\forall \eta, 3 \leq v \leq \bar{v}$$
.

where  $\Omega$  is a sufficiently large positive number.

Upon obtaining the optimal solution  $(a_v^*, b_v^*, c_v^*, d_v^*)$  of the RoCoF linearization model, the nonlinear location based RoCoF constraints (11) can be converted into linear constraints in SCUC:  $4*(\bar{v}-1)$  inequalities (15) that ensures  $t_{\bar{v}-1}$  is maximum, along with the RoCoF threshold constraints  $t_{\bar{v}-1} \leq RoCoF_{lim}$ .

# IV. SCUC FORMULATIONS

SCUC is to determine the day-ahead generation scheduling for each synchronous generator and each hour. Traditionally, the SCUC model does not consider any frequency constraints, which may lead to severe system instability issue for lowerinertia power grid with substantial amount of renewable generation. In this section, we first present the traditional SCUC (T-SCUC) model, the ERC-SCUC model and the proposed LRC-SCUC model; they all minimize the system cost subject to various constraints. Subsequently, we will describe the proposed VI-LRC-SCUC model that utilize virtual inertia.

Objective function (16a) is shared by three SCUC models: T-SCUC, ERC-SCUC and LRC-SCUC. It is to minimize the total system cost consisting of variable fuel costs, no-load costs, start-up costs, and reserve costs.

The T-SCUC model includes various constraints (16b)-(160). Equation (16b) enforces the nodal power balance. Network power flows are calculated in (16c) and are restricted by the transmission capacity as shown in (16d). The scheduled energy production and generation reserves are bounded by unit generation capacity and ramping rate (16e)-(16j). As defined in (16h), the reserve requirements ensure the reserve is sufficient to cover any loss of a single generator. The start-up status and on/off status of conventional units are defined as binary variables (16k)-(16o).

$$\begin{split} \min_{\Phi} \sum\nolimits_{g \in G} \sum\nolimits_{t \in T} (c_{g} P_{g,t} + c_{g}^{NL} u_{g,t} + c_{g}^{SU} v_{g,t} \\ + c_{g}^{RE} r_{g,t}) \end{split} \tag{16a}$$

$$\sum_{g \in G} P_{g,t} + \sum_{k \in K(n-)} P_{k,t} - \sum_{k \in K(n+)} P_{k,t} - d_{n,t} + E_{n,t}$$
(16b)

$$=0, \forall n, t,$$

$$P_{k,t} - b_k (\theta_{n,t} - \theta_{m,t}) = 0, \ \forall k, t, \tag{16c}$$

$$-P_k^{max} \le P_{k,t} \le P_k^{max}, \ \forall k, t, \tag{16d}$$

$$P_g^{min}u_{g,t} \le p_{g,t}, \qquad \forall g, t, \tag{16e}$$

$$P_{g,t} + r_{g,t} \le u_{g,t} P_g^{max}, \qquad \forall g, t, \tag{16f}$$

$$0 \le r_{g,t} \le R_g^{re} u_{g,t}, \qquad \forall g,t, \tag{16g} \label{eq:16g}$$

$$\sum_{j \in G} r_{j,t} \ge p_{g,t} + r_{g,t}, \qquad \forall g, t, \tag{16h}$$

$$P_{g,t} - P_{g,t-1} \le R_g^h, \qquad \forall g, t, \tag{16i}$$

$$P_{g,t-1} - P_{g,t} \le R_g^h, \qquad \forall g, t, \tag{16j}$$

$$v_{a,t} \ge u_{a,t} - u_{a,t-1} \quad \forall g, t, \tag{16k}$$

$$v_{g,t+1} \le 1 - u_{g,t} \quad \forall g, t \le nT - 1,$$
 (161)

$$v_{g,t} \le u_{g,t} \quad \forall g, t,$$
 (16m)

$$v_{g,t} \in \{0,1\}, \quad \forall g, t,$$
 (16n)

$$u_{a,t} \in \{0,1\}, \qquad \forall g, t, \tag{160}$$

As mentioned before, the ERC-SCUC model is constrained to guarantee generator frequency stability considering the relative location to the potential G-1 contingency. Loss of synchronous generation would lead to a reduction in total system inertia which would cause a higher RoCoF comparing to the event with no synchronous inertia loss. The system RoCoF limit following a G-1 contingency is guaranteed by applying the following set of frequency related constraints (16p)-(16r). (16p) defines the rated power of dispatched generators, while

(16q) calculates the system synchronous inertia, and (16r) ensures the system frequency security.

$$k_{g,t} = P_g^{max} u_{g,t}, \qquad \forall \ g \ , t, \tag{16p}$$

$$M_t = \frac{\sum_{j \in G} 2H_j k_{j,t}}{\omega_0}, \quad \forall t,$$
 (16q)

$$RoCoF_{lim}(M_t - \frac{2H_g k_{g,t}}{\omega_0})\omega_0 \ge p_{g,t} \quad \forall g, t,$$
 (16r)

If the generation scheduling is not appropriately constrained to reflect the G-1 contingency and distinct locational frequency, unexpected tripping of RoCoF relays and cascading contingency may take place. To address this issue, squared Fiedler mode amplitude  $\beta_{2b}^2$  is introduced in this paper to assess the impact of disturbance, a power loss at bus b, on frequencies in the whole grid. Considering the inter oscillation between regions which may cause unexpected tripping of RoCoF relays [27], we create two locational RoCoF constraints in this paper based on the definition of local buses and non-local buses. Constraint (16s) defines the average nodal inertia over generator buses and (16t) calculates the change in average nodal inertia due to loss of a generator. Constraint (16u) imposes the limit on locational RoCoF of local buses under possible G-1 contingency while (16v) ensures the locational frequency security on non-local buses.

Intry on non-local buses. 
$$m_{t} = \frac{\sum_{j \in G} 2H_{j}k_{j,t}}{N\omega_{0}}, \quad \forall t, \qquad (16s)$$

$$\Delta m_{g,t} = \frac{2H_{g}k_{g,t}}{N\omega_{0}}, \quad \forall g,t, \qquad (16t)$$

$$\frac{p_{g,t}e^{-\gamma\frac{T_{1}}{2}}(1-e^{-\gamma\Delta t})}{2N(m_{t}-\Delta m_{g,t})\pi\gamma\Delta t} + \frac{p_{g,t}e^{-\gamma\frac{T_{1}}{2}}}{2\pi m_{t}t} \frac{\beta_{2n}\beta_{2b}}{\sqrt{\frac{\lambda_{2}}{(m_{t}-\Delta m_{g,t})} \frac{\gamma^{2}}{4}\Delta t}}$$

$$\left[e^{-\gamma\frac{\Delta t}{2}}\sin\left(\sqrt{\frac{\lambda_{2}}{(m_{t}-\Delta m_{g,t})} - \frac{\gamma^{2}}{4}}(T_{1} + \Delta t)\right) - \right] \leq RoCoF_{lim}, \qquad (16u)$$

$$\forall n \in N_{l}, g, t, \qquad \frac{p_{g,t}e^{-\gamma\frac{T_{2}}{2}}(1-e^{-\gamma\Delta t})}{2N(m_{t}-\Delta m_{g,t})\pi\gamma\Delta t} + \frac{p_{g,t}e^{-\gamma\frac{T_{2}}{2}}}{2\pi m_{g,t}t} \frac{\beta_{2n}\beta_{2b}}{\sqrt{\frac{\lambda_{2}}{(m_{t}-\Delta m_{g,t})} \frac{\gamma^{2}}{4}\Delta t}}$$

$$\left[-\frac{\lambda_{2}}{\sqrt{2}}\right] = \frac{\lambda_{2}}{\sqrt{2}} \frac{\gamma^{2}}{\sqrt{2}} \left(\frac{\pi}{2}\right)$$

$$\left[e^{-\gamma \frac{\Delta t}{2}} \sin \left(\sqrt{\frac{\lambda_2}{(m_t - \Delta m_{g,t})} - \frac{\gamma^2}{4}} (T_2 + \Delta t)\right) - \sin \left(\sqrt{\frac{\lambda_2}{(m_t - \Delta m_{g,t})} - \frac{\gamma^2}{4}} T_2\right)\right]$$

$$\leq RoCoF_{lim},$$

$$\forall n \in N_{nl}, g, t,$$
(16v)

RESs such as wind power and solar power require converters to connect to the grid. There are different implementations for synchronous machine response emulation. The study in [28] shows that control schemes can be utilized to provide equivalent inertia through non-synchronous devices. Such concept introduces techniques like virtual inertia emulation to mimic the behavior of synchronous machines, displacing the inertia provided by synchronous generators with cheap inertia ancil-

lary service provided by various resources such as virtual synchronous machine. It is also noted that the virtual inertia requires fast responsive energy buffer; the kinetic energy in a wind turbine and the energy in a battery are limited energy resources for virtual inertia responses. To study the effect of virtual inertia on the power grid, a virtual inertia involved location based RoCoF constrained SCUC model or a VI-LRC-SCUC model is proposed and examined in this paper. Compared to (16a), this model also considers the cost for virtual inertia provision; the updated objective function for the proposed VI-LRC-SCUC model is shown in (17a). Moreover, when virtual inertia is considered, constraints (16q)-(16r) should be replaced by (17b)-(17c). Expression (17b) describes the system inertial response respect to aggregate inertia contributions from condensers and inverter-based resources. (17c) defines the change in average nodal inertia while virtual inertia is applied.

$$min \sum_{g \in G} \sum_{t \in T} (c_g P_{gt} + c_g^{NL} u_{gt} + c_g^{SU} v_{gt} + c_g^{RE} r_{g,t}) + \sum_{t \in T} c^{VI} M_t^{VI}$$
(17a)

$$RoCoF_{lim}(M_t + M_t^{VI} - \frac{2H_g k_{g,t}}{\omega_0})\omega_0 \ge p_{g,t}, \quad \forall g, t, \quad (17b)$$

$$m_t = \frac{\sum_{j \in G} 2H_j k_{j,t}}{N\omega_0} + \frac{M_t^{VI}}{N}, \quad \forall t,$$
 (17c)

It is also practical to set a limit on the total virtual inertia due to budget limit and resource limit. This limit should also be considered as follows,

$$M_t^{VI} \le M_t^{Total}, \quad \forall t,$$
 (17d)

This paper examines five different SCUC models that are summarized in Table I. In this table, the objective functions and constraints enforced are listed for each SCUC model.

TABLE I SCUC formulation under different models

Model	Objective Function	Shared Constraints	Unique Constraints
T-SCUC ERC-SCUC LRC-SCUC	(16a)		None (16p)-(16r) (16p), (16s)-(16v)
VI-ERC-SCUC	(17a)	(16b)-(16o)	(16p)-(16q), (17b), (17d)
VI-LRC-SCUC	(17a)		(16p), (16t)-(16v), (17c)-(17d)

Note that non-linear constraints (16u) and 16(v) are linearized with the PWL method described in Section III before solving the associated SCUC models.

#### V. CASE STUDIES

# A. Test System Description

In this paper, the IEEE 24-bus system is used to demonstrate the effectiveness of the proposed LRC-SCUC and VI-LRC-SCUC models [29]. This test system contains 24 buses, 38 generators and 38 lines, which also considers decarbonized generation characterized by wind power and solar power on generator buses. Fig. 3 shows the renewable generation and load profile for a system scenario with 60% of maximum renewable energy penetration level during peak hour. Electricity demand ranges from 1,432 MW to a peak of 3,222 MW. Regarding post-contingency frequency limits, RoCoF must be below 0.5Hz/s to avoid the tripping of RoCoF-sensitive pro-

tection relays. The mathematical models are implemented in Python using Pyomo [30]-[31] and solved with the Gurobi solver [32]. The computer with Intel® Xeon(R) W-2195 CPU @ 2.30GHz and 128 GB of RAM was utilized to conduct the numerical simulations.

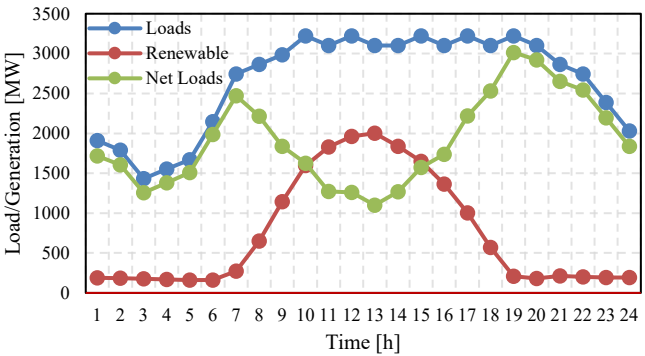


Fig. 3. Renewable generation and load profile of the IEEE 24-bus system.

### B. Investigation of Frequency Propagation

In this subsection, we analyze the implications of a generation loss in scenarios with different system inertia. Based on the RoCoF expression that is the left-hand side terms of (11), we numerically calculated RoCoF at t = 0s and  $\Delta t = 0.1$ s for local bus 21 that is illustrated in Fig. 4 where the loss of largest unit is considered.

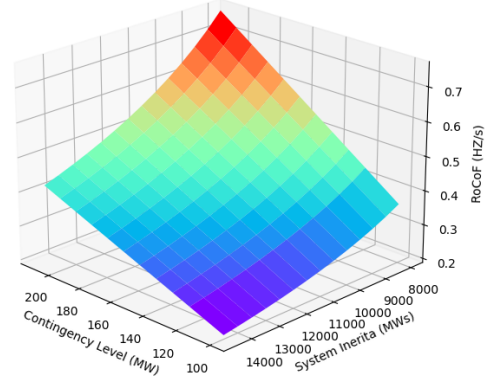


Fig. 4. RoCoF of local bus 21 at t = 0s and  $\Delta t = 0.1$ s following a G-1 contingency on bus 18.

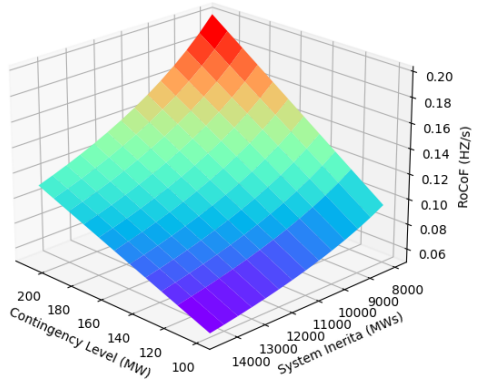


Fig. 5. RoCoF of non-local bus 1 at t = 0s and  $\Delta t = 0.1$ s following G-1 contingency on bus 18.

As shown Fig. 5, generators on non-local bus 1 with opposite Fiedler mode would experience a much smaller RoCoF than local bus 18 at t = 0s. Local buses substantially suffer much higher RoCoF than non-local buses under the same disturbance at t = 0s. The preliminary results indicate that larger

RoCoF originates from local buses with larger amplitude of the Fielder mode of the system Laplacian matrix L. Hence, the generators on local buses with large Fiedler mode are more likely to violate the RoCoF limits during the initial period following a G-1 contingency.

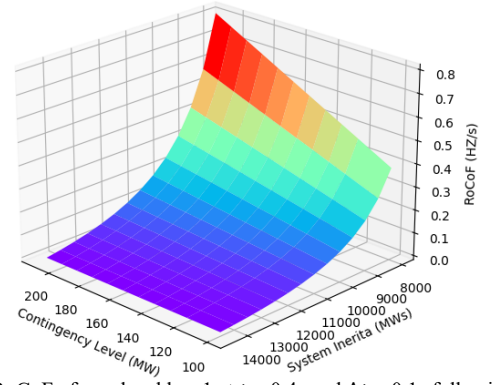


Fig. 6. RoCoF of non-local bus 1 at t = 0.4s and  $\Delta t = 0.1$ s following G-1 contingency on bus 18.

Fig. 6 shows the numerically calculated RoCoF of non-local bus 1 at t=0.4s and  $\Delta t=0.1$ s under the same scenario. It is observed from Fig. 6 that the RoCoF on non-local buses at t=0.4s is secured within the safe range when system inertia is high, which is not the case when t=0s. It is important to note that when system inertia drops below a certain threshold the RoCoF increases drastically especially for the buses have relatively large Fiedler mode absolute value. This subsection demonstrates the effect of inertia and Fiedler mode value on locational RoCoF: with higher system inertia, the amplitude of the oscillation decreases especially for non-local buses with large Fiedler mode absolute value.

## C. LRC-SCUC Model

In this section, we first conduct the simulation of T-SCUC model for 24-hour period, which serves as a benchmark to show the impact of frequency constraints. To ensure the system G-1 stability, the ERC-SCUC and LRC-SCUC models are secured against the loss of largest generation. The evaluation point and the PWL segments are set with  $\eta=3$  and  $\bar{v}=4$ . It takes 95.61s for the T-SCUC model while it decreases to 20.91s for ERC-SCUC model. For the proposed LRC-SCUC model, the computing time is 75.45s indicating that the proposed LRC-SCUC model can be efficiently solved with less time than T-SCUC.

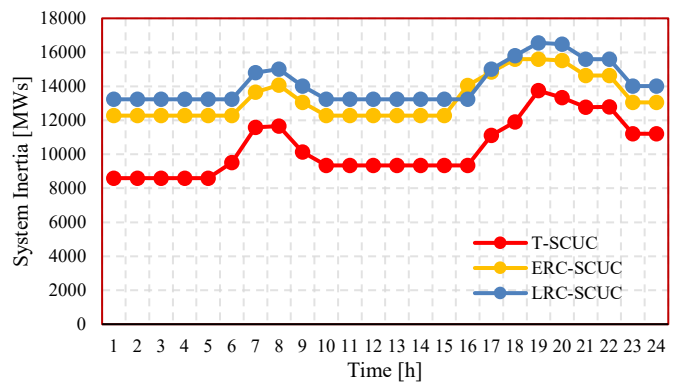


Fig. 7. Impact of RoCoF constraints on the total system inertia.

The aggregate system inertia over the scheduling horizon is depicted in Fig. 7. When net load increases during the period

of hours 5-8 and hours 16-20, the total system aggregate inertia increases as well in all three cases. The inertia of committed synchronous generators based on T-SCUC model is lower than the other two SCUC models where RoCoF constraints are included. The total system synchronous inertia of the proposed LRC-SCUC model is the highest which reflects the impact of locational RoCoF constraints.

Some other insightful conclusions can also be drawn from Fig. 7. When net load decreases dramatically between hours 9-11 due to the increase of RES generation, the system aggregate inertia in T-SCUC case drops significantly, implying larger frequency deviation and higher RoCoF under a fault instance. While system inertia maintains relatively high level in the case of LRC-SCUC. To investigate how commitment scheduling impacts the system frequency dynamics following *G*-1 contingency, we conduct time-domain simulations with all three models at peak hour 12 on Transient Security Analysis Tools (TSAT) following the loss of largest generator [33].

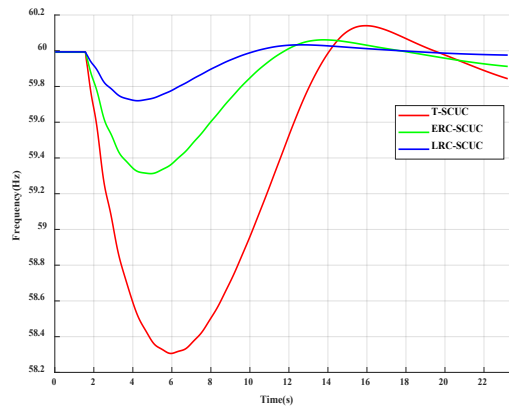
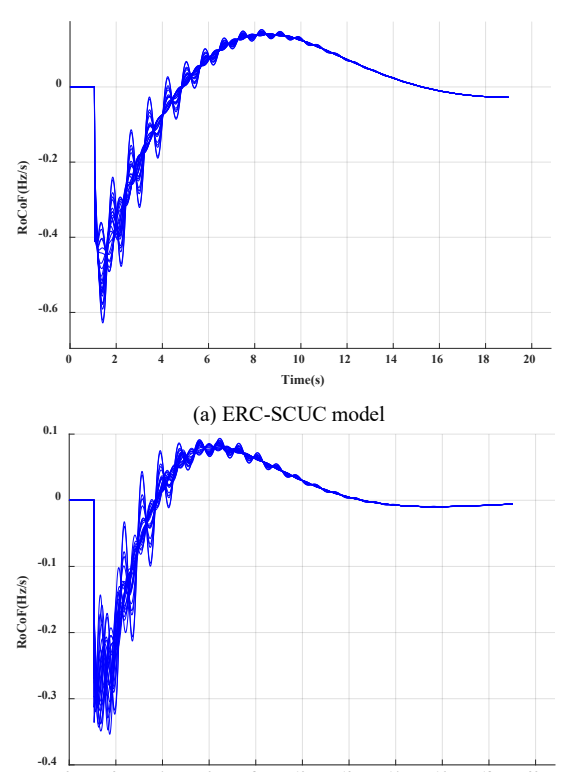


Fig. 8. System frequency response after loss of the generator with the largest generation at hour 12.

The time-domain frequency response curves of the system with T-SCUC, ERC-SCUC and LRC-SCUC models under the loss of the largest generation are plotted in Fig. 8. Results show that for the T-SCUC model without any RoCoF constraints, the loss of the largest committed generation of 400 MW on bus 22 leads to the largest frequency excursion, imposing potential trigger of the RoCoF relays. For ERC-SCUC model, the system is secured against a loss of largest generation at 182.9 MW on the same bus. Understandably, the frequency excursion is significantly reduced, while the system frequency nadir is improved from 58.30 Hz to 59.33 Hz. In the third case with the solution from the proposed LRC-SCUC model being implemented, the largest generation is on bus 23 and the potential largest G-1 contingency level is further reduced to 155 MW, which is about 5% of largest demand, leading to the least frequency excursion at 59.74 Hz.

The RoCoF of all buses following the loss of largest generation is depicted for ERC-SCUC and LRC-SCUC in Fig. 9. For the T-SCUC model without RoCoF constraints, following the event of a loss of 400MW generation on bus 22, the RoCoFs on all buses violate the prescribed system limit by a large margin ranging from 0.97 Hz/s to 1.45 Hz/s. For ERC-SCUC model, the highest COI RoCoF can be numerically calculated as -0.48 Hz/s which is less than the limit. However, the highest locational RoCoFs still violate the prescribed RoCoF limit which reflects that impact of inter-area oscillations cannot be handled well by ERC-SCUC model. For the

generator commitment and dispatch solution obtained with the proposed LRC-SCUC model, the highest locational RoCoF is only -0.35 Hz/s, meeting the RoCoF security requirement. This demonstrates the performance of the proposed LRC-SCUC model in terms of limiting locational RoCoFs at different locations.



(b) LRC-SCUC model.

Fig. 9. RoCoF of all buses following the loss of largest generation in different cases.

TABLE II SCUC costs [\$] under different models

Model	Total	Start-up	Operation	Reserves
T-SCUC	891,391	56,704	744,973	89,714
ERC-SCUC	988,524	59,462	881,633	47,429
LRC-SCUC	1,050,989	66,810	955,983	28,196

Table II compares system total operational costs with and without frequency related constraints. By adding system equivalent model based RoCoF constraints, the total generation cost increases from \$891,391 to \$988,524 indicating that the additional system inertia constraints lead to a 10.9% increase in total system cost. In the presence of location based RoCoF constraints, an increase of 17.90% in total operational cost is observed. On the other hand, the reserve cost decreases largely as the largest scheduled generation decreases. Meanwhile, additional synchronous machines are committed to cover the shortage of inertia to limit locational RoCoFs following the loss of largest generation, which accordingly increases the operation cost as well as the start-up cost.

Furthermore, Fig. 10 compares the average unit inertia (AUI) of committed generators during the whole dispatch horizon. A noticeable large value of AUI between hours 1-5 and hour 16-18 are monitored in T-SCUC and ERC-SCUC cases. Larger AUI means that generators with larger rated

power and synchronous inertia are scheduled in the system operation, implying larger potential *G*-1 contingency level. While the AUI of proposed LRC-SCUC case is relatively stable, it can be inferred that committing distributed synchronous generators can decrease the level of a *G*-1 contingency, thus enhancing the resilience of the system despite a changing mix of generation.

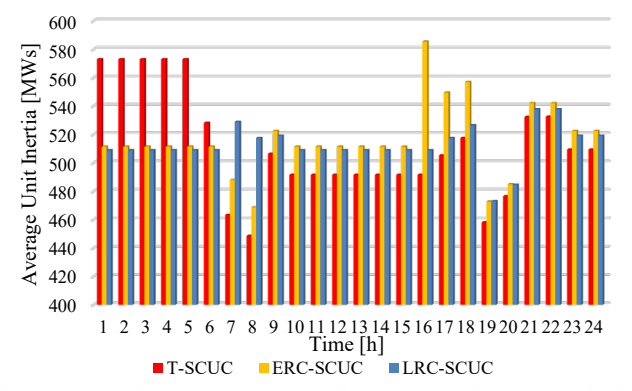


Fig.10. Impact of RoCoF constraints on the average unit inertia contribution.

#### D. Sensitivity Analysis on RES Penetration Levels

The sensitivity analysis with different renewable penetration levels is conducted in this subsection. Following the daily load profile shown in Fig. 3, four scenarios are considered for different RES penetration levels during peak hour from 20% to 80% with an increment of 20%. Given the system peak load is 3,222 MW at hour 12, the corresponding RES generations during peak hour are 644.4 MW, 1,288.8 MW, 1,933.2 MW and 2,577.6 MW respectively.

Table III presents the total system inertia at peak hour 12 in different RES penetration level scenarios. As shown in Table III, when RES penetration level increases from 20% to 80%, the synchronous inertia of committed synchronous generators based on T-SCUC drops significantly comparing to the LRC-SCUC model.

TABLE III
System inertia [MWs] under different models at hour 12

M - 1-1	RES Penetration Level			
Model	20%	40%	60%	80%
T-SCUC	11,706	10,434	9,342	7,792
ERC-SCUC	14,639	13,063	12,275	10,880
LRC-SCUC	15,599	14,503	13,235	13,095

TABLE IV Highest RoCOF [Hz/s] monitored under different scenarios at hour 12

Model	RES Penetration Level			
	20%	40%	60%	80%
T-SCUC	1.26	1.32	1.45	1.65
ERC-SCUC	0.74	0.65	0.63	0.61
LRC-SCUC	0.30	0.34	0.35	0.38

One may be interested to compare the nodal frequency performance of the three SCUC models. Simulations have been conducted in TSAT considering loss of largest generation at peak hour 12. Table IV shows the highest RoCoF monitored on generator buses following the *G*-1 contingency under different scenarios. It can be observed that highest RoCoF in both ERC-SCUC and T-SCUC cases violates the limit which may subsequently trip frequency-sensitive protection relays, while

the RoCoFs are within the prespecified safe range in all cases with the proposed LRC-SCUC model.

TABLE V SCUC costs [\$] under different models

-	Model	RES Penetration Level			
	Model	20%	40%	60%	80%
	T-SCUC	1,357,203	1,077,439	891,391	750,199
	ERC-SCUC	1,459,983	1,181,493	988,524	845,606
	LRC-SCUC	1,546,833	1,253,221	1,050,989	908,353

The costs with those three SCUC models are listed in Table V. Obviously, incorporating frequency related RoCoF constraints in SCUC leads to an increase of system total generation cost in all scenarios. The change in the cost is dependent on the change in penetration level of renewable resources.

#### E. Influence of Virtual Inertia

In this subsection, the proposed VI-LRC-SCUC model that considers virtual inertia  $M_t^{VI}$  is implemented and the effects of virtual inertia on day-ahead scheduling and system stability are examined. The total available virtual inertia is considered to be 2,000 MWs in this paper. To evaluate the influence of including virtual inertia based RoCoF constraints in SCUC models, we analyzed the market results of five models that are averaged over all 24 hours.

TABLE VI Average LMP with different SCUC models

Model	Average LMP [\$/MWh]	Average congestion LMP [\$/MWh]	Energy LMP [\$/MWh]
T-SCUC	37.56	23.31	14.25
ERC-SCUC	41.44	24.20	17.24
VI-ERC-SCUC	40.41	23.17	17.24
LRC-SCUC	45.89	29.09	16.80
VI-LRC-SCUC	37.88	21.08	16.80

The average locational market price (LMP) defined in [34], including energy component and congestion component is presented in Table VI. With virtual inertia implemented, the average LMP is the same for ERC-SCUC and VI-ERC-SCUC. The proposed VI-LRC-SCUC model provides better results than other models, the average congestion LMP decreases from 29.09 \$/MWh to 21.08 \$/MWh when virtual inertia is included, the average LMP decreases considerably from 45.89 \$/MWh to 37.88 \$/MWh, which implies that virtual inertia ancillary services can significantly improve the market efficiency when locational RoCoF constraints are included in the day-ahead scheduling SCUC model.

TABLE VII
Market results (averaged over 24 hour) with different SCUC models

Model	Load payment [\$/h]	Generator revenue [\$/h]	Generator cost [\$/h]	Generator rent [\$/h]	Congestion revenue [\$/h]
T-SCUC	80,476	72,589	37,141	35,448	7,887
ERC- SCUC	82,975	59,651	41,189	18,462	23,324
VI-ERC- SCUC	83,202	62,005	40,475	21,530	21,197
LRC- SCUC	127,770	52,882	43,791	9,091	74,888
VI-LRC- SCUC	81,112	61,827	43,315	18,512	19,285

According to the market results in Table VII, the congestion revenue is relatively low for T-SCUC and ERC-SCUC com-

paring to the proposed LRC-SCUC model. This indicates that with location based RoCoF constraints, network congestion contributes more to the differences in nodal LMPs and leads to an increase of load payment. When virtual inertia is introduced, the load payment drops significantly for the proposed LRC-SCUC model, as well as the congestion revenue. It is interesting to observe although VI-ERC-SCUC achieves a lower cost than ERC-SCUC, its load payment is even higher.

#### VI. CONCLUSIONS

In this paper, the concept of locational frequency security is introduced. We first investigate the impact of Fiedler mode on locational frequency dynamics, and then define the expression of locational frequency dynamics considering *G*-1 contingency in multi-machine systems. Utilizing PWL techniques, the highly non-linear location based RoCoF constraints are linearized before being incorporated into the proposed LRC-SCUC and VI-LRC-SCUC models.

Simulation results show that the inclusion of location based RoCoF constraints in the SCUC model can ensure the locational frequency security during *G*-1 contingency events. Such frequency-related constraints also significantly affect the scheduling of synchronous generators and consequently the expected system cost. By implementing virtual inertia, the system congestion revenue and load payment can be largely reduced, implying that the proposed VI-LRC-SCUC model can improve the market efficiency.

#### REFERENCES

- [1] H. Gu, R. Yan, and T. K. Saha, "Minimum synchronous inertia requirement of renewable power systems," IEEE Trans. Power Syst., vol. 33, no. 2, pp. 1533–1543, Mar. 2017.
- [2] Y. Liu, S. You, and Y. Liu, "Study of wind and PV frequency control in U.S. power grids—EI and TI case studies," IEEE Power Energy Technol. Syst. J., vol. 4, no. 3, pp. 65–73, Sep. 2017.
- [3] F. Milano, F. D"orfler, G. Hug, D. J. Hill, and G. Verbi"c, "Foundations and challenges of low-inertia systems," in Power Systems Computation Conference (PSCC), Jun 2018.
- [4] Energy Emergencies Executive Committee, "GB power system disruption on 9 August 2019," 2019. [Online]. Available: https://assets.publishing.service.gov.uk/government/uploads/system/uploads/attachment\_data/file/855767/e3c-gb-power-disruption-9-august-2019-final-report.pdf.
- [5] A. Crivellaro, A. Tayyebi, C. Gavriluta, D. Groß, A. Anta, F. Kupzog and F. Dörfler, "Beyond low-inertia systems: Massive integration of grid-forming power converters in transmission grids," 2020 IEEE Powe & Energy Society General Meeting (PESGM), Montreal, QC, Aug, 2020.
- [6] J. Matevosyan and P. Du, "Wind integration in ERCOT," in Integration of Large-Scale Renewable Energy into Bulk Power Systems. Springer, 2017, pp. 1-25.
- [7] Jun Cao, Wenjuan Du, Haifeng Wang and Malcolm McCulloch, "Optimal Sizing and Control Strategies for Hybrid Storages System as Limited by Grid Frequency Deviations," *IEEE Trans. Power Syst.*, vol. 33, no. 5, pp. 5486-5495, Feb. 2018.
- [8] Vincenzo Trovato, Agnès Bialecki and Anes DallagiDemand, "Unit Commitment with Inertia-Dependent and Multispeed Allocation of Frequency Response Services," *IEEE Trans. Power Syst.*, vol. 34, no. 2, pp. 1537-1548, March. 2019.
- [9] J Riesz, J Gilmore, and I MacGill, "Frequency Control Ancillary Service Market Design: Insights from the Australian National Electricity Market," Elect. J., vol. 28, no. 3, pp. 86–99, 2015.
- [10] EirGrid and SONI, "DS3 System Services: Review TSO Recommendations," EirGrid, Dublin, Ireland, Tech. Rep., May 2013
- [11] EirGrid and SONI, "Operational Constraints Update," EirGrid, Tech. Rep., March 2019

- [12] M. Paturet, U. Markovic, S. Delikaraoglou, E. Vrettos, P. Aristidou and G. Hug, "Economic Valuation and Pricing of Inertia in Inverter-Dominated Power Systems". [Master thesis]
- [13] T. Borsche and F. Dorfler, "On placement of synthetic inertia with explicit time-domain constraints," May 2017. [Online]. Available: https://arxiv.org/pdf/1705.03244.pdf.
- [14] A Adrees, JV Milanović and P Mancarella, "Effect of Inertia Heterogeneity on Frequency Dynamics of Low-inertia Power Systems," *IET Generc., Transmiss. Distrib.*, vol. 13, no. 14, pp. 2951–2958, Jul. 2019.
- [15] Phillip M. Ashton, Christopher S. Saunders, Gareth A. Taylor, Alex M. Carter and Martin E. Bradley, "Inertia Estimation of the GB Power System Using Synchrophasor," *IEEE Transactions on Power Systems*. vol. 30, no. 2, pp. 701-709, March. 2015.
- [16] Bala Kameshwar Poolla, Saverio Bolognani and Florian Dörfler, "Optimal Placement of Virtual Inertia in Power Grids," *IEEE Transactions on Automatic Control*. vol. 62, no. 12, pp. 6209-6220, Dec. 2017.
- [17] Matthieu Paturet, Uros Markovic, Stefanos Delikaraoglou, Evangelos Vrettos, Petros Aristidou and Gabriela Hug, "Stochastic Unit Commiment in Low-Inertia Grids," *IEEE Trans. Power Syst.*, vol. 35, no. 5, pp. 3448-3458, Sept. 2020.
- [18] F. D"orfler and F. Bullo, "Kron reduction of graphs with applications to electrical networks," *IEEE Trans. Circuits Syst. I: Regular Papers* vol. 60, no. 1, pp. 150–163, Jan. 2013.
- [19] Mingjian Tuo, and Xingpeng Li, "Optimal Allocation of Virtual Inertia Devices for Enhancing Frequency Stability in Low-Inertia Power Systems", in *Proc.* 53<sup>rd</sup> North Amer. Power Symp., Nov. 2021, accepted
- [20] L. Pagnier and P. Jacquod, "Inertia location and slow network modes determine disturbance propagation in large-scale power grids," *PLoS ONE* 14, e0213550 (2019).
- [21] Bahman Alinezhad Osbouei, Gareth A. Taylor, Olivier Bronckart, Johan Maricq and Martin Bradley, "Impact of Inertia Distribution on Power System Stability and Operation," 2019 IEEE Milan Power-Tech, Milan, Italy, June. 2019.
- [22] Turaj Amraee, Mohammad Ghaderi Darebaghi, Alireza Soroudi and Andrew Keane, "Probabilistic Under Frequency Load Shedding Considering RoCoF Relays of Distributed Generators," *IEEE Trans. Pow*er Syst., vol. 33, no. 4, pp. 3587-3598, July. 2018.
- [23] Luis Badesa, Fei teng, and Goran Strbac, "Conditions for Regional Frequency Stability in Power System Scheduling-Part I: Theory," IEEE Trans. Power Syst., Early Access.
- [24] P. W. Sauer and M. A. Pai, Power System Dynamics and Stability. Upper Saddle River, NJ, USA: Prentice-Hall, 1998.
- [25] Mingjian Tuo, and Xingpeng Li, "Dynamic Estimation of Power System Inertia Distribution Using Synchrophasor Measurements", in Proc. 52nd North Amer. Power Symp., April. 2021, virtually, Tempe, AZ, USA, pp. 1–6.
- [26] H. Ahmadi and H. Ghasemi, "Security-constrained unit commitment with linearized system frequency limit constraints," *IEEE Trans. Power Syst.*, vol. 29, no. 4, pp. 1536-1545, Jul. 2014.
- [27] M. Tyloo, L. Pagnier, and P. Jacquod, "The key player problem in complex oscillator networks and electric power grids: Resistance centralities identify local vulnerabilities," Sci. Adv., vol. 5, no. 11, 2019, Art. No eaaw8359.
- [28] Federico Milano, and Álvaro Ortega, "A Method for Evaluating Frequency Regulation in an Electrical Grid Part I: Theory," *IEEE Trans. Power Syst.*, vol. 36, no. 1, pp. 183-193, Jan. 2021.
- [29] Arun Venkatesh Ramesh, Xingpeng Li, and Kory W Hedman, "An accelerated-decomposition approach for security-constrained unit commitment with corrective network reconfiguration," *IEEE Trans. Power Syst.*, July. 2021, Early Access.
- [30] Hart, William E., Jean-Paul Watson, and David L. Woodruff. "Pyomo: modeling and solving mathematical programs in Python." Mathematical Programming Computation 3, no. 3 (2011): 219-260.
- [31] Hart, William E., Carl Laird, Jean-Paul Watson, David L. Woodruff, Gabriel A. Hackebeil, Bethany L. Nicholson, and John D. Siirola. Pyomo – Optimization Modeling in Python. Springer, 2017.
- [32] Gurobi Optimization Inc. Gurobi optimizer reference manual. http://www.gurobi.com/, 2014.
- [33] DSA Tools Power Labs Inc., British Columbia, Canada, 2011.
- [34] Xingpeng Li and Kory W. Hedman, "Enhanced energy management system with corrective transmission switching – Part I: Methodology," *IEEE Trans. Power Syst.*, vol. 34, no. 6, pp. 4490-4502, Nov. 2019.